

# GeSn/Ge heterostructure short-wave infrared photodetectors on silicon

A. Gassenq,<sup>1,2,\*</sup> F. Gencarelli,<sup>3</sup> J. Van Campenhout,<sup>3</sup> Y. Shimura,<sup>3</sup> R. Loo,<sup>3</sup>  
G. Narcy,<sup>4</sup> B. Vincent,<sup>3</sup> and G. Roelkens<sup>1,2</sup>

<sup>1</sup>Photonics Research Group, INTEC Department, Ghent University-IMEC, Sint-Pietersnieuwstraat 41, 9000 Ghent, Belgium

<sup>2</sup>Center for Nano- and Biophotonics (NB-Photonics), Ghent University, Belgium

<sup>3</sup>imec, Kapeldreef 75, 3001 Leuven, Belgium

<sup>4</sup>Institut d'Electronique du Sud (IES), UMR 5214, Université Montpellier 2 - CNRS, F-34095 Montpellier cedex 5, France

\*alban.gassenq@intec.ugent.be

**Abstract:** A surface-illuminated photoconductive detector based on Ge<sub>0.91</sub>Sn<sub>0.09</sub> quantum wells with Ge barriers grown on a silicon substrate is demonstrated. Photodetection up to 2.2 μm is achieved with a responsivity of 0.1 A/W for 5V bias. The spectral absorption characteristics are analyzed as a function of the GeSn/Ge heterostructure parameters. This work demonstrates that GeSn/Ge heterostructures can be used to develop SOI waveguide integrated photodetectors for short-wave infrared applications.

©2012 Optical Society of America

OCIS codes: (130.0130) Integrated optics; (040.3060) Infrared; (040.0040) Detectors.

---

## References and links

1. J. Menéndez and J. Kouvetakis, "Type-I Ge/Ge<sub>1-x-y</sub>Si<sub>x</sub>Sn<sub>y</sub> strained-layer hetero-structures with a direct Ge Bandgap," *Appl. Phys. Lett.* **85**(7), 1175–1177 (2004).
2. G. Sun, R. A. Soref, and H. H. Cheng, "Design of a Si-based lattice-matched room-temperature GeSn/GeSiSn multi-quantum-well mid-infrared laser diode," *Opt. Express* **18**(19), 19957–19965 (2010).
3. F. Gencarelli, B. Vincent, L. Souriau, O. Richard, W. Vandervorst, R. Loo, M. Caymax, and M. Heyns, "Low-temperature Ge and GeSn Chemical Vapor Deposition using Ge<sub>2</sub>H<sub>6</sub>," *Thin Solid Films* **520**(8), 3211–3215 (2012).
4. F. Gencarelli, B. Vincent, J. Demeulemeester, A. Vantomme, A. Moussa, A. Franquet, A. Kumara, J. Meersschaut, W. Vandervorst, R. Loo, M. Caymax, K. Temst, and M. Heyns, "Crystalline Properties and Strain Relaxation Mechanism of CVD Grown GeSn," *ECS Trans.* (to be published).
5. J. G. Crowder, S. D. Smith, A. Vass, and J. Keddle, "Infrared methods for gas detection," in *Mid-Infrared Semiconductor Optoelectronics* (Springer, 2006).
6. A. Gassenq, N. Hattasan, L. Cerutti, J. B. Rodriguez, E. Tournié, G. Roelkens, and G. Roelkens, "Study of evanescently-coupled and grating-assisted GaInAsSb photodiodes integrated on a silicon photonic chip," *Opt. Express* **20**(11), 11665–11672 (2012).
7. L. Vivien, A. Polzer, D. Marris-Morini, J. Osmond, J. M. Hartmann, P. Crozat, E. Cassan, C. Kopp, H. Zimmermann, and J. M. Fédéli, "Zero-bias 40Gbit/s germanium waveguide photodetector on silicon," *Opt. Express* **20**(2), 1096–1101 (2012).
8. R. Roucka, R. Beeler, J. Mathews, M. Y. Ryu, Y. Kee Yeo, J. Menendez, and J. Kouvetakis, "Complementary metal-oxide semiconductor-compatible detector materials with enhanced 1550 nm responsivity via Sn-doping of Ge/Si(100)," *J. Appl. Phys.* **109**(10), 103115 (2011).
9. J. Werner, M. Oehme, A. Schirmer, E. Kasper, and J. Schulze, "Molecular beam epitaxy grown GeSn p-i-n photodetectors integrated on Si," *Thin Solid Films* **520**(8), 3361–3364 (2012).
10. S. Su, B. Cheng, C. Xue, W. Wang, Q. Cao, H. Xue, W. Hu, G. Zhang, Y. Zuo, and Q. Wang, "GeSn p-i-n photodetector for all telecommunication bands detection," *Opt. Express* **19**(7), 6400–6405 (2011).
11. G. E. Chang, S. W. Chang, and S. L. Chuang, "Strain-Balanced Ge<sub>z</sub>Sn<sub>1-z</sub>-Si<sub>x</sub>Ge<sub>y</sub>Sn<sub>1-x-y</sub> Multiple-Quantum-Well Lasers," *IEEE J. Quantum Electron.* **46**(12), 1813–1820 (2010).
12. C. G. Van de Walle, "Band lineups and deformation in the model-solid theory," *Phys. Rev. B* **39**(3), 1871–1883 (1989).
13. M. Krijn, "Heterojunction band offsets and effective masses in III-V quaternary alloys," *Semicond. Sci. Technol.* **6**(1), 27–31 (1991).
14. G. Sun, R. A. Soref, and H. H. Cheng, "Design of a Si-based lattice-matched room-temperature GeSn/GeSiSn multi-quantum-well mid-infrared laser diode," *Opt. Express* **18**(19), 19957–19965 (2010).

15. J. Menéndez and J. Kouvetakis, "Type-I Ge/Ge<sub>1-x-y</sub>Si<sub>x</sub>Sn<sub>y</sub> strained-layer heterostructures with a direct Ge Bandgap," *Appl. Phys. Lett.* **85**(7), 1175–1177 (2004).
16. V. R. D'Costa, J. Tolle, J. Xie, J. Menéndez, and J. Kouvetakis, "Transport properties of doped GeSn alloys," *AIP Conf. Proc.* **1199**, 57–58 (2008).
17. R. Soref, J. Hendrickson, and J. W. Cleary, "Mid- to long-wavelength infrared plasmonic-photonics using heavily doped n-Ge/Ge and n-GeSn/GeSn heterostructures," *Opt. Express* **20**(4), 3814–3824 (2012). <http://www.ioffe.rssi.ru/SVA/NSM/Semicond/Ge/>
18. <http://www.ioffe.rssi.ru/SVA/NSM/Semicond/Ge/>
19. B. Vincent, F. Gencarelli, H. Bender, C. Merckling, B. Douhard, D. H. Petersen, O. Hansen, H. H. Henrichsen, J. Meersschat, W. Vandervorst, M. Heyns, R. Loo, and M. Caymax, "Undoped and in-situ B doped GeSn epitaxial growth on Ge by atmospheric pressure-chemical vapor deposition," *Appl. Phys. Lett.* **99**(15), 152103 (2011).
20. J. Zeng and L. Hanssen, "Calibration of the spectral radiant power responsivity of windowed pyroelectric radiometers from 785 nm to 14 μm," *Proc. SPIE* **7082**, 70820Y (2008).
21. R. Roucka, J. Xie, J. Kouvetakis, J. Mathews, V. D'Costa, J. Menéndez, J. Tolle, and S.-Q. Yu, "Ge<sub>1-y</sub>Sn<sub>y</sub> photoconductor structures at 1.55 μm: From advanced materials to prototype devices," *J. Vac. Sci. Technol. B* **26**(6), 1952–1960 (2008).
22. C. J. Kim, H. S. Lee, Y. J. Cho, K. Kang, and M. H. Jo, "Diameter-dependent internal gain in ohmic Ge nanowire photodetectors," *Nano Lett.* **10**(6), 2043–2048 (2010).
23. E. Monroy, F. Calle, J. L. Pau, E. Munoz, F. Omnes, B. Beaumont, and P. Gibart, "AlGaIn-based UV photodetectors," *J. Cryst. Growth* **230**(3–4), 537–543 (2001).
24. R. Roucka, J. Mathews, R. T. Beeler, J. Tolle, J. Kouvetakis, and J. Menéndez, "Direct gap electroluminescence from Si/Ge<sub>1-y</sub>Sn<sub>y</sub> p-i-n heterostructure diodes," *Appl. Phys. Lett.* **98**(6), 061109 (2011).
25. J. Mathews, R. T. Beeler, J. Tolle, C. Xu, R. Roucka, J. Kouvetakis, and J. Menéndez, "Direct-gap photoluminescence with tunable emission wavelength in Ge<sub>1-y</sub>Sn<sub>y</sub> alloys on silicon," *Appl. Phys. Lett.* **97**(22), 221912 (2010).
26. G. He and H. A. Atwater, "Interband Transitions in Sn<sub>x</sub>Ge<sub>1-x</sub> Alloys," *Phys. Rev. Lett.* **79**(10), 1937–1940 (1997).
27. H. Lin, R. Chen, W. Lu, Y. Huo, T. I. Kamins, and J. S. Harris, "Investigation of the direct band gaps in Ge<sub>1-x</sub>Sn<sub>x</sub> alloys with strain control by photoreflectance spectroscopy," *Appl. Phys. Lett.* **100**(10), 102109 (2012).

## 1. Introduction

Silicon (Si) and Germanium (Ge) are the dominant materials for electronic and photonic integrated circuits. However, the indirect bandgap of these group IV elements prevents them from being used to realize efficient light-emitting components. Therefore, the interest in the GeSiSn material system has significantly increased over the last few years. In theory, a direct energetic transition in such a heterostructure grown on a Si substrate can be realized [1,2] by growing lattice matched or tensile strained GeSn alloys. In this article, we investigate compressively strained GeSn on Ge, which, while lacking a direct band gap, also exhibits interesting optical absorption properties in order to realize short-wave infrared photodetectors. Even though the lattice mismatch between Ge and Sn is large, recent progress in growth has been reported, showing the realization of a fully strained Ge<sub>0.92</sub>Sn<sub>0.08</sub> layer on Ge [3,4]. This technological development allows evaluating the emission and absorption properties of these lattice-matched heterostructures. In this paper we demonstrate the use of a GeSn/Ge heterostructure-based photodetector in the short-wave infrared (SWIR) wavelength range, which is very attractive for several applications. For instance, the field of spectroscopic sensing relies on the strong gas/liquid/solid absorption features in this wavelength range [5]. By waferbonding GaInAsSb/GaSb photodiodes on top of silicon waveguide circuits, photonic integrated circuits are now being developed for applications in the 2–2.5 μm wavelength range [6]. However, combined with the recent progress in the integration of Ge photodetectors on Silicon-On-Insulator (SOI) for telecom-band applications [7], GeSn-based integrated photodetectors can become an attractive approach for monolithically integrated SWIR photodetectors. Moreover, recent results show that adding Sn in the p-i-n Ge detector matrix also increases the responsivity of the detector in the telecom wavelength range and extends the cut-off wavelength beyond 1.7 μm [8–10]. In this paper, we present photoconductive detectors based on a highly strained Ge<sub>0.91</sub>Sn<sub>0.09</sub>/relaxed Ge heterostructure grown on silicon with a cut-off wavelength of 2.4 μm.

## 2. Band structure analysis

Figure 1(a) shows the evolution of the band parameters of  $\text{Ge}_{1-x}\text{Sn}_x$  between Ge and strained Sn grown on Ge. The unstrained parameters for Sn extracted from [11] are presented in the dashed box. By taking into account the effect of the strain in the Krijn-Van de Walle model [12,13], the compressive strain in the Sn splits the valence band and shifts the conduction band towards higher energy. By applying the unstrained bowing parameters, we find a bandgap still dominated by the L-valley, which is not the case for the unstrained GeSn alloys [14,15]. Nevertheless, a clear red-shift of the material absorption edge as a function of increasing Sn-content can be observed. The following energy level dependencies on Sn-content were obtained:  $E_{c,\Gamma}(x) = 0.89 - 1.08x + 1.94x^2$  eV,  $E_{c,L}(x) = 0.76 - 0.67x + 1.23x^2$  eV,  $E_{hh}(x) = 0.1 + 1.26x$  eV and  $E_{lh}(x) = 0.1 + 0.85x$  eV. From the band parameters presented in Fig. 1(a), the band diagram and the energy levels in quantum-confined structures can be calculated. Figure 1(b) presents the typical Ge/GeSn lattice-matched epitaxial stack discussed in this work. In this example, a strained  $\text{Ge}_{0.9}\text{Sn}_{0.1}$  quantum well with a thickness of 20nm is embedded in relaxed Ge. The calculated energy levels in the quantum well are presented by the dashed lines together with their respective carrier probability distribution. The effective masses are extracted from [16–18] except for the GeSn hole masses, which are to our knowledge currently unknown. Since the heavy holes are well confined in the GeSn quantum well, the actual mass has little influence on the energy level, while this is strongly the case for the light holes, making that there is some uncertainty on the light hole energy level. However, because of the high compressive strain, the absorption is dominated by the heavy holes. The light hole energy levels are only presented on Fig. 1(b) to illustrate the transitions at higher photon energies, but will depend strongly on the actual effective mass. While Fig. 1(b) indicates different sub-energy levels for the different types of carriers, since the energy difference between them is on the order of  $kT$  at room temperature, these will not give rise to individual absorption features in the absorption characteristics of the photodetector. The effective bandgaps are estimated to be 0.59eV with respect to the  $\Gamma$ -valley and 0.49eV with respect to the L-valley. In this work, the influence of the quantum well thickness and the Sn-content will be experimentally studied.

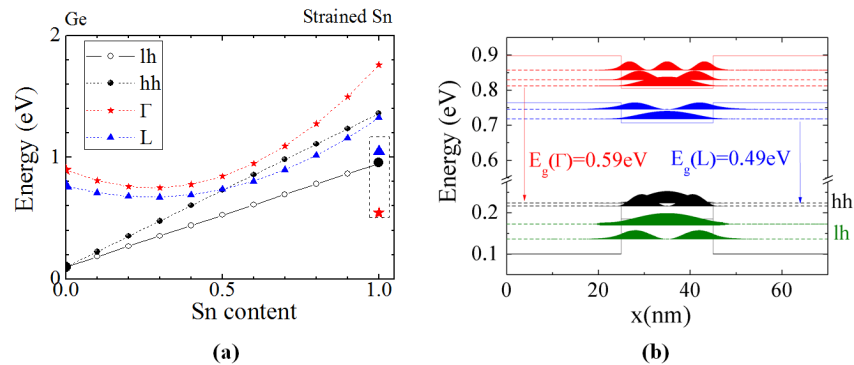


Fig. 1. Room temperature modeling of (a) Band parameters of  $\text{Ge}_{1-x}\text{Sn}_x$  lattice-matched to Ge; (b) Band diagram and carrier presence probability for a  $\text{Ge}_{0.9}\text{Sn}_{0.1}/\text{Ge}$  heterostructure (20nm thick quantum well). The quantum well energy levels are illustrated by the dashed lines.

## 3. Photodetector fabrication

The GeSn/Ge heterostructures are grown by atmospheric pressure chemical vapor deposition using an ASM Epsilon-like EPI reactor on a 200mm (001) Si substrate with a relaxed Ge buffer ( $\sim 0.5\mu\text{m}$  thick). GeSn quantum wells were grown separated by 100nm thick Ge barriers. The GeSn growth conditions are reported in [3] and [19]. Measured by X-ray diffraction (XRD), up to 9% Sn content can be reached. Figure 2(a) shows an example of

XRD measurements together with the modeling done by the software “Philips X-pert Epitaxy” for a  $\text{Ge}_{0.91}\text{Sn}_{0.09}$  heterostructure (a single 25nm thick quantum well with a 100nm thick Ge cap layer). The XRD measurements reveal a lattice-matched  $\text{Ge}_{0.91}\text{Sn}_{0.09}$  layer on Ge with periodic fringes illustrating the abrupt Ge/GeSn interfaces. The Si substrate is also visible on the measurement with a linewidth narrower than that of the Ge because the thickness of the Ge relaxed buffer is only 0.5 $\mu\text{m}$ . Comparing with the modeling of the layers on a Ge substrate, we obtain a good correlation, showing a high crystallographic quality of the GeSn/Ge heterostructure.

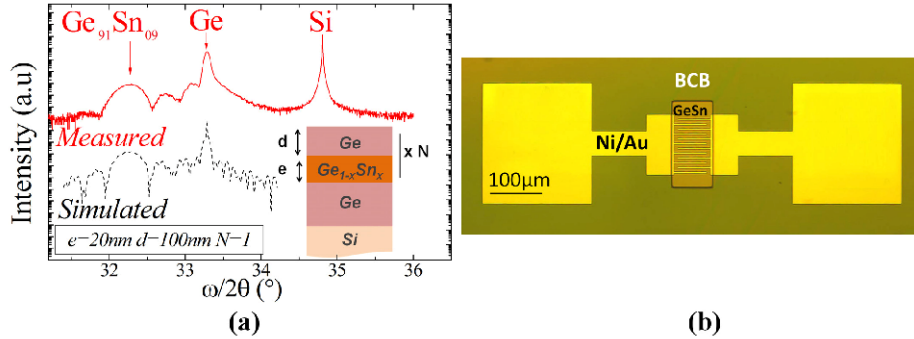


Fig. 2. (a) Measured (solid line) and simulated (dashed line) XRD rocking curve of the epitaxial stack with a 25nm  $\text{Ge}_{0.91}\text{Sn}_{0.09}$  strained quantum well on Ge with a 100nm Ge cap layer; The generalized layer stack is shown in the inset; (b) Top view of the processed GeSn photoconductive detector for surface illumination.

In order to study the GeSn absorption in the near-infrared and short-wave infrared wavelength range, photoconductive detectors were processed in these epitaxial layer stacks. Figure 2(b) presents a top view of a realized photodetector. Interdigitated electrodes with 2 $\mu\text{m}$  wide fingers separated from each other by 6 $\mu\text{m}$  are connected to two independent contact pads. Only the combs are in contact with the sample because the pads are isolated from the epitaxial stack by a DVS-BCB spacer layer. The process starts with the photolithography of the DVS-BCB (4022-25) followed by an annealing step at 250 $^{\circ}\text{C}$  for 2 hours. The BCB exposure time is voluntarily increased to obtain a sloped DVS-BCB profile for improved electrode coverage. The electrodes are defined using a lift-off process. Electron-gun evaporation was used to deposit the electrodes, consisting of 10nm Ni and 200nm Au.

#### 4. Photodetector characterization

Fourier Transform InfraRed (FTIR) based calibrated measurements were done to assess the spectral responsivity [20]. First, the light from the internal tungsten halogen source of our FTIR spectrometer was modulated in a Michelson interferometer with one moving mirror and focused on the photoconductive detector by a set of gold mirrors. The photoconductors were driven with a current of 0.2mA and the voltage drop over the photoconductor was sent back to the FTIR electrical input to calculate the spectral dependence of the responsivity (in arbitrary units). For the calibration in A/W, another measurement was done using surface illumination of the photodetector using several fiber coupled sources: a red LED ( $\lambda \sim 0.7\mu\text{m}$ ), semiconductor lasers (1.3 and 1.55 $\mu\text{m}$ , 1.7 $\mu\text{m}$ ) and a Cr:ZnSe laser (2.1-2.4 $\mu\text{m}$ ). Figure 3(a) presents the current versus voltage characteristic of different realized photoconductors in the dark. In sample A, a 45nm  $\text{Ge}_{0.91}\text{Sn}_{0.09}$  layer was grown on top of the Ge buffer. For sample B, N  $\text{Ge}_{0.91}\text{Sn}_{0.09}$  quantum wells (N = 0,1,2,3) with a thickness of 20nm were grown, separated by 100nm Ge barriers. From this graph it is clear that when the top surface is GeSn (sample A on the Fig. 3(a)), the dark current strongly increases as a function of applied voltage. However, when a Ge cap layer is used on top of the GeSn/Ge hetero-structure (sample B on the Fig. 3(a)), the dark conductivity of the structure is much lower. For this

reason, Ge cap layers were used to develop photoconductive detectors with GeSn quantum wells. Figure 3(b) shows the measured current versus voltage characteristic as a function of the optical power in the fiber at  $1.55\mu\text{m}$  for a Ge photoconductive detector (sample B with  $N = 0$  on the Fig. 3(a)). Under illumination, the series resistance dramatically changes from a dark resistivity of  $12\text{k}\Omega$  to  $2.2\text{k}\Omega$  under illumination with  $3\text{mW}$  optical power. This already shows an improved conductivity compared to earlier developed GeSn photoconductive devices [21]. A nonlinear relation between photocurrent and optical power can be observed, which is often observed in photoconductive detectors [22,23]: the responsivity increases when the input power decreases until it reaches  $1.5\text{A/W}$  (for a  $5\text{V}$  bias) at  $0.1\text{mW}$  optical input power.

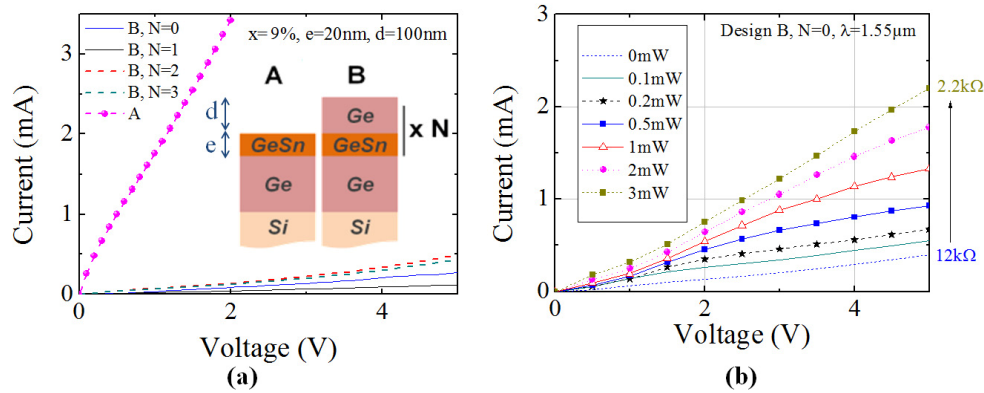


Fig. 3. I(V) measurements of processed photoconductive detectors: (a) dark current for sample A without Ge cap layer and sample B with  $N = 0, 1, 2$  or  $3$   $\text{Ge}_{0.91}\text{Sn}_{0.09}$  quantum wells; (b) under  $1.55\mu\text{m}$  illumination for a Ge photoconductive detector.

Figure 4 presents the normalized detector responsivities (measured with an FTIR) as a function of the wavelength for different GeSn/Ge designs. This measurement allows assessing the intrinsic absorption features of the GeSn/Ge structure. The influence of the number of GeSn quantum wells on the detector responsivity spectral dependence can be seen in Fig. 4(a). The  $\text{Ge}_{0.91}\text{Sn}_{0.09}$  quantum wells with a thickness of  $20\text{nm}$  are separated by  $100\text{nm}$  Ge barriers. Photodetection for photon energies below the  $\Gamma$ -bandgap of Ge is only possible when GeSn quantum wells are present in the structure. Photodetection up to  $2.4\mu\text{m}$  is obtained. In the structure with 3 quantum wells, two energetic transitions in the absorption spectrum can be observed. This level discretization is also observed in the absorption spectrum of the  $\text{Ge}_{0.92}\text{Sn}_{0.08}/\text{Ge}$  structures with 3 quantum wells presented in Fig. 4(b). These quantum wells have a thickness of  $20$  or  $13\text{nm}$  and are separated by  $25\text{nm}$  of Ge. In this case, the lower Sn-content and a super lattice effect due to the coupling of the quantum wells result in a higher photon energy cut-off compared to Fig. 4(a). Figure 4(c) presents the responsivity spectrum of one  $40\text{nm}$  quantum well as a function of the Sn content. In this case, the state density is closer to a continuum and the discretization of the state density is not observed. However, the bandgap values can be measured to be at  $0.63\text{eV}$  for  $\text{Ge}_{0.95}\text{Sn}_{0.05}$  and  $0.57\text{eV}$  for  $\text{Ge}_{0.92}\text{Sn}_{0.08}$ . Due to the strain, these observed bandgaps are slightly higher compared to unstrained GeSn alloys [24–27].

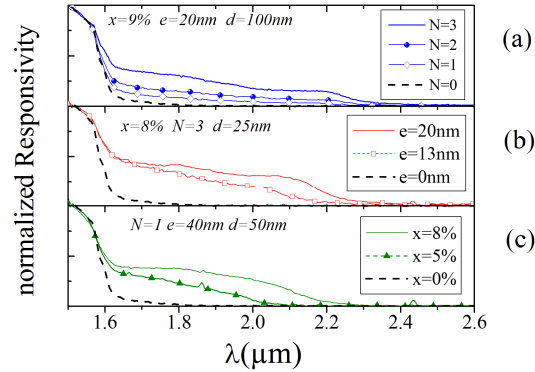


Fig. 4. Normalized detector responsivity as function of wavelength for GeSn/Ge photoconductive detectors: (a) with 1, 2 or 3  $\text{Ge}_{0.91}\text{Sn}_{0.09}$  quantum wells with a thickness of 20nm; (b) with 3  $\text{Ge}_{0.92}\text{Sn}_{0.08}$  quantum wells with a thickness of 13 or 20nm; (c) for a single quantum well with a thickness of 40nm with different Sn content.

In order to implement the photodetectors in a short-wave infrared system, measurements of the absolute responsivity in A/W at a fixed 5V bias were carried out using several calibrated fiber coupled sources. As previously presented, the samples B (Fig. 3(a)) were grown with  $N = 0, 1, 2$  or 3  $\text{Ge}_{0.91}\text{Sn}_{0.09}$  quantum wells. Figure 5 presents the responsivity versus wavelength, the solid lines referring to the FTIR characterization method and the dots corresponding to the calibration with several sources at 5V bias (for 1mW optical input power). Higher responsivities are obtained when the number of GeSn quantum wells is increased. The best responsivities are reported for the structure with 3 quantum wells at the wavelength of 0.75, 1.5, 1.75 and 2.2 $\mu\text{m}$  with respectively 2A/W, 1A/W, 0.3A/W and 0.1A/W. These high responsivities illustrate the good quality of the highly strained  $\text{Ge}_{0.91}\text{Sn}_{0.09}$  quantum wells on Ge. Higher responsivities can even be envisaged when using a waveguide-coupled GeSn photodetector, since in this case the responsivity is decoupled from the actual absorber thickness, which is limited in this case.

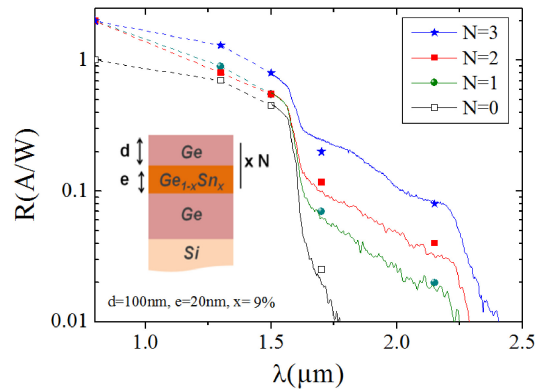


Fig. 5. Responsivity as a function of wavelength at 5V bias for structures with 0,1,2 or 3  $\text{Ge}_{0.91}\text{Sn}_{0.09}$  quantum wells embedded in Ge. The dots are measured using surface illumination with a fiber-coupled source and the solid lines are extracted from FTIR-based measurements.

Nevertheless, the sensitivity of the photoconductive detector in a practical system is limited by the device dark current. In order to improve the sensitivity, a lock-in detection system can be used. A photodetector bandwidth above 2MHz was observed for these devices, which is sufficient to remove the 1/f noise contribution in the dark current noise spectral density. Another approach that can be envisaged is the incorporation of these GeSn quantum

wells in a Ge-based p-i-n (waveguide based) photodetector, which in recent years has been implemented for pure Ge detectors for telecom applications [7]. From this work, we can conclude that GeSn-based detectors are a serious candidate for short-wave infrared photodetection in silicon photonic integrated circuits.

## **5. Conclusion**

In this article, photoconductive detectors based on highly strained  $\text{Ge}_{0.91}\text{Sn}_{0.09}$  quantum wells were investigated. Compared to Ge photoconductive detectors, an improvement of the responsivity is reported over the whole wavelength range from 0.75  $\mu\text{m}$  to 2.4  $\mu\text{m}$ . This allows envisioning integrated GeSn/Ge photodetectors on Si waveguides by selective growth for near-infrared and short-wave infrared applications. These GeSn photodetectors can also be used to precisely extract GeSn material constants, based on the measured absorption spectrum.

## **Acknowledgments**

Y. Shimura acknowledges the FWO for an FWO Pegasus Marie Curie fellowship. Part of this work was carried out in the framework of the FP7-ERC-MIRACLE project.